Transfer matrix method for the analysis of space-time-modulated media and systems

Junfei Li,[1,*] Xiaohui Zhu,[2,*] Chen Shen,[1] Xiuyuan Peng,[1] and Steven A. Cummer[1,†]
[1]*Department of Electrical and Computer Engineering, Duke University, Durham, North Carolina 27708, USA*
[2]*School of Mechatronics Engineering, Harbin Institute of Technology, Harbin, Heilongjiang 150001, China*

(Received 7 June 2019; revised manuscript received 15 October 2019; published 31 October 2019)

Space-time modulation adds another powerful degree of freedom to the manipulation of classical wave systems. It opens the door for complex control of wave behavior beyond the reach of stationary systems, such as nonreciprocal wave transport and realization of gain media. Here we generalize the transfer matrix method and use it to create a general framework to solve wave propagation problems in time-varying acoustic, electromagnetic, and electric circuit systems. The proposed method provides a versatile approach for the study of general space-time-varying systems, which allows any number of time-modulated elements with an arbitrary modulation profile, facilities the investigation of high-order modes, and provides an interface between space-time-modulated systems and other systems.

DOI: 10.1103/PhysRevB.100.144311

I. INTRODUCTION

Wave propagation in systems where the material parameters or structures are varying in both space and time has attracted considerable attention in recent years. Such space-time modulation provides an efficient means to break time-reversal symmetry and has found many applications in the field of integrated circuits (ICs), optics, electromagnetics (EM), and acoustics. For example, time-varying transmission lines (TVTLs) have been used to create frequency converters, multipliers, and nonreciprocal devices such as isolators and circulators [1–9]. Recently, the idea of achieving nonreciprocity through space-time modulation has been applied to modern optical and electromagnetic systems [10–22]. For mechanical waves, space-time-modulated elastic beams have been proposed to create a directional band gap [23,24]. Space-time-modulated mass-spring systems have also been proposed to study directional wave manipulation for elastic waves [25,26]. In airborne acoustics, frequency converters and parametric amplifiers have been demonstrated in a space-time-modulated metamaterial [27]. Acoustic isolators [28], circulators [29–31], and topological insulators [32] have also been demonstrated with temporally modulated resonators.

Theoretical tools available for studying time-varying wave systems generally fall into several categories. In time-varying transmission lines [1–3], the most commonly used approach is to directly solve the coupled differential equations by assuming a slowly varying envelope and then solve the coupled equations for the envelope. However, such an approach considers only a small number of interacting waveguide modes and neglects all the higher-order modes. Taking these modes into account will result in additional coupled differential equations and make the system more difficult to solve efficiently. Space-time Floquet theory [23,25,33], on the other hand, calculates the band structure for an infinitely long system. However, the Floquet theory predicts only which waveguide modes are coupled, and it does not provide detailed information on how waves change gradually in such systems. Both theoretical approaches deal with infinitely long and continuous systems. However, in practice, the systems must have a finite length, and in many cases, the realization for space-time-modulated media is discretized [9,24,26,27]. Furthermore, both solving coupled wave equations directly and space-time Floquet theory deal with wave propagation where the material properties are modulated sinusoidally, and they cannot be applied to more complicated modulation profiles. For discrete systems with space-time-varying boundary conditions, the system can be solved by balancing the harmonics at each order [14,28]. Another type of discrete system involves one or more coupled resonators and is generally solved by the coupled mode theory (CMT) [34,35]. CMT has been widely applied in mechanical-optical systems [16,19,36] and was recently introduced in acoustics [30,31]. However, the coupling coefficients are usually not easy to determine or design in practice. Furthermore, for both harmonic balancing and CMT, as the number of resonators or boundaries increases and with the increase of modes taken into account, the coupled equations become complicated to solve.

Here we propose a generalized transfer matrix approach for solving one-dimensional space-time-varying systems. By setting up time-varying boundary conditions and rewriting them into transfer matrix form, the effects of time variation are localized. Therefore, all the time-varying components can be described individually so that we can calculate a system with an arbitrary number of time-varying elements and an arbitrary spatial modulation profile by simply multiplying their transfer matrices. It is shown that with a small number of elements, it reduces to the harmonic balancing method described in [28], while with a large number of modulated elements with small spacing, it reduces to the continuous counterpart [27] and space-time Floquet theory [23,25,33]. The results are verified with finite-difference time-domain (FDTD) simulations. Our

*These authors contributed equally to this work.
†Corresponding author: cummer@ee.duke.edu

approach provides a versatile platform to investigate the behavior of general space-time-modulated systems. Compared with current available theoretical tools, it has a number of advantages. First, it handles multiple higher-order waves and arbitrary number of modulated elements without increasing the computational complexity, therefore providing a better approximation. Second, it offers many degrees of freedom and thus allows the study of arbitrary modulation parameters such as modulation depth and phase for each element or even the study of a system with random time modulation, which is difficult for other approaches. Third, it has no constraint for the element spacing or material properties. Therefore, it facilities the study of the interplay of time-dependent wave behavior with other classical behaviors, such as resonances, multiple scattering, and inhomogeneity. Fourth, by representing the whole system with a transfer matrix, our method provides an interface for the study of interaction between a space-time-modulated system and other stationary and nonstationary systems.

This paper is organized as follows. First, we present the formulation of the transfer matrix method for general time-varying systems. We use acoustic representation, and the results can be directly applied to EM waves and ICs, and the corresponding formulation can be found in Appendix A. The approach is then applied to several examples to show its capabilities and advantages. In the first case, we present the design of an acoustic diode without operating at resonance frequencies. The isolation level can be controlled by employing different numbers of modulated resonators and modulation strategies. The off-resonance feature makes the design robust to loss and fabrication errors. In the second case, we will show that when the phase-matching condition is met, parametric mode conversion and amplification can be achieved with multiple space-time-modulated resonators. With this example, we will discuss the impact of high-order modes, multiple scattering, and how this approach reduces to continuous theory and space-time Floquet theory under several conditions.

II. MATRIX REPRESENTATION OF A SPACE-TIME-VARYING SYSTEM

In this section, we exemplify the derivation with the acoustic representation. The general procedure applies to the study of EM waves and ICs, where one just needs to substitute the pressure and velocity (p, v) with electric and magnetic fields (E, H) or voltage and current (V, I). The details for the EM and IC formulation and the corresponding realization approaches are summarized in Appendix A.

A. Response of a time-varying load in series

Consider an acoustic waveguide loaded with a time-varying impedance sheet Z_L. Assume the modulation amplitude is sufficiently small and the impedance is varying harmonically in the form of

$$Z_L(\omega, t) = Z_{L0}(\omega)[1 + a\cos(\Omega t + \phi)], \tag{1}$$

where Ω is the modulation frequency, ϕ is the initial phase of the modulation, a denotes the modulation depth ($a \ll 1$), and $Z_{L0}(\omega)$ is the impedance without modulation. In general, a can be a function of frequency depending on the physical parameters under modulation. A plane wave is launched into the waveguide with angular frequency ω_0. We would like to note here that the impedance is defined in the frequency domain; such a treatment shall be valid under the slow and weak modulation. However, as is shown in later sections, such a treatment yields great agreement between the calculation and simulation even when the modulation frequency is twice the input frequency. Due to the time-varying load impedance, harmonics will be generated. Therefore, the pressure and velocity upstream and downstream of the load are written as

$$p_{\mp} = \sum_{n=-\infty}^{\infty} p_{\mp}^n e^{j\omega_n t}, \tag{2}$$

$$v_{\mp} = \sum_{n=-\infty}^{\infty} v_{\mp}^n e^{j\omega_n t}, \tag{3}$$

where $\omega_n = \omega_0 \pm n\Omega$. The boundary condition at the position of the load should satisfy

$$p_- - p_+ = \sum_{n=-\infty}^{\infty} Z_L^n v_+^n e^{j\omega_n t}, \tag{4}$$

$$v_- = v_+, \tag{5}$$

where the superscript denotes the impedance at each order of harmonic, i.e., $Z_L^n = Z_L(\omega_n, t)$ and so on. Putting the expression of the series load, pressure, and velocity into Eqs. (4) and (5) and equating the terms with $e^{j\omega_n t}$ using the relation $\cos(\Omega t + \phi) = \frac{1}{2}[e^{j(\Omega t+\phi)} + e^{-j(\Omega t+\phi)}]$, we can rewrite the boundary conditions in terms of each order of the harmonics:

$$p_-^n - p_+^n = Z_{L0}^n v_+^n + \frac{aZ_{L0}^{n-1}}{2} e^{j\phi} v_+^{n-1} + \frac{aZ_{L0}^{n+1}}{2} e^{-j\phi} v_+^{n+1}, \tag{6}$$

$$v_-^n = v_+^n, \tag{7}$$

where $Z_{L0}^n = Z_{L0}(\omega_n)$. The transfer matrix M is defined as

$$\begin{bmatrix} \vdots \\ p_-^{n-1} \\ v_-^{n-1} \\ p_-^n \\ v_-^n \\ p_-^{n+1} \\ v_-^{n+1} \\ \vdots \end{bmatrix} = M \begin{bmatrix} \vdots \\ p_+^{n-1} \\ v_+^{n-1} \\ p_+^n \\ v_+^n \\ p_+^{n+1} \\ v_+^{n+1} \\ \vdots \end{bmatrix}. \tag{8}$$

With the boundary conditions, the transfer matrix at the load can be written as

$$M = \begin{bmatrix} & \vdots & \vdots & \vdots & \vdots & \vdots & \vdots & \\ \dots & 1 & Z_{L0}^{n-1} & 0 & \frac{aZ_{L0}^n}{2} e^{-j\phi} & 0 & 0 & \dots \\ \dots & 0 & 1 & 0 & 0 & 0 & 0 & \dots \\ \dots & 0 & \frac{aZ_{L0}^{n-1}}{2} e^{j\phi} & 1 & Z_{L0}^n & 0 & \frac{aZ_{L0}^{n+1}}{2} e^{-j\phi} & \dots \\ \dots & 0 & 0 & 0 & 1 & 0 & 0 & \dots \\ \dots & 0 & 0 & 0 & \frac{aZ_{L0}^n}{2} e^{j\phi} & 1 & Z_{L0}^{n+1} & \dots \\ \dots & 0 & 0 & 0 & 0 & 0 & 1 & \dots \\ & \vdots & \vdots & \vdots & \vdots & \vdots & \vdots & \end{bmatrix}. \tag{9}$$

For waves traveling in an empty waveguide, the transfer matrix can be simply written as

$$M_T = \begin{bmatrix} & \vdots & \vdots & \vdots & \\ \dots & M_T^{n-1} & 0 & 0 & \dots \\ \dots & 0 & M_T^{n} & 0 & \dots \\ \dots & 0 & 0 & M_T^{n+1} & \dots \\ & \vdots & \vdots & \vdots & \end{bmatrix}, \tag{10}$$

where

$$M_T^i = \begin{bmatrix} \cos(k_i d) & jZ_0 \sin(k_i d) \\ \frac{j}{Z_0}\sin(k_i d) & \cos(k_i d) \end{bmatrix} \quad (i = \dots, n-1, n, n+1, \dots). \tag{11}$$

Here Z_0 is the characteristic impedance of air, k_i is the wave number for the ith-order wave, and d is the length of the waveguide. All the coupling terms between each order are zero since the waveguide is stationary.

For a system composed of N equally spaced cascaded time-varying impedance sheets, the transfer matrix can be calculated as $M_{tot} = M_1 M_T M_2 M_T \cdots M_T M_N$, where M_i $(i = 1, \dots, N)$ denotes the transfer matrix of the impedance loads and M_T is the transfer matrix of each section of the empty waveguide.

B. Response of a time-varying load in parallel

For a shunted load on the waveguide, it is more convenient to use the effective admittance, defined as $Y_L = S_L/(S_w Z_L)$, where S_w and S_L denote the cross-sectional areas of the waveguide and the load, respectively. Note here that the admittance is scaled by the ratio between the cross-sectional areas to keep the generality of our formulation. Now we assume the admittance varies in the form of $Y_L(\omega, t) = Y_{L0}(\omega)[1 + a\cos(\Omega t + \phi)]$. In this case, the boundary condition at the position of the load should satisfy

$$p_- = p_+, \tag{12}$$

$$v_- - v_+ = \sum_{n=-\infty}^{\infty} Y_L^n p_+^n e^{j\omega_n t}. \tag{13}$$

The boundary conditions for each order then become

$$p_-^n = p_+^n, \tag{14}$$

$$v_-^n - v_+^n = Y_{L0}^n p_+^n + \frac{aY_{L0}^{n-1}}{2} e^{j\phi} p_+^{n-1} + \frac{aY_{L0}^{n+1}}{2} e^{-j\phi} p_+^{n+1}, \tag{15}$$

where the superscript denotes the admittance at each order of harmonic, i.e., $Y_{L0}^n = Y_{L0}(\omega_n)$. In this case, the transfer matrix at the load becomes

$$M = \begin{bmatrix} & \vdots & \vdots & \vdots & \vdots & \vdots & \vdots & \\ \dots & 1 & 0 & 0 & 0 & 0 & 0 & \dots \\ \dots & Y_{L0}^{n-1} & 1 & \frac{aY_{L0}^{n}}{2} e^{-j\phi} & 0 & 0 & 0 & \dots \\ \dots & 0 & 0 & 1 & 0 & 0 & 0 & \dots \\ \dots & \frac{aY_{L0}^{n-1}}{2} e^{j\phi} & 0 & Y_{L0}^{n} & 1 & \frac{aY_{L0}^{n+1}}{2} e^{-j\phi} & 0 & \dots \\ \dots & 0 & 0 & 0 & 0 & 1 & 0 & \dots \\ \dots & 0 & 0 & \frac{aY_{L0}^{n}}{2} e^{j\phi} & 0 & Y_{L0}^{n+1} & 1 & \dots \\ & \vdots & \vdots & \vdots & \vdots & \vdots & \vdots & \end{bmatrix}. \tag{16}$$

We can see from Eqs. (9) and (16) that the loads in series and in parallel are similar, which is consistent with the passive cases [37]. With the transfer matrix for the loads and empty waveguide, the transfer matrix for the entire structure can be calculated by multiplying the transfer matrices for all components. Hence, the transmission and reflection coefficients can be calculated by converting the transfer matrix into a scattering matrix. The conversion from the transfer matrix to the scattering matrix is given in Appendix B.

With the transfer matrix method we can, in principle, take all the orders of harmonics into account. However, in practice, the matrix shall be truncated to account only for the orders that are non-negligible. Compared with existing theories that characterize space-time-modulated systems, there are three main advantages for the proposed method. First, our proposed transfer matrix method takes higher-order modes into account. It will be shown in the following sections that these high-order modes exhibit non-negligible effects on the wave propagation. Second, current theories focus on the traveling-wave-like modulation where the modulation has a linear phase gradient along the space, while with the proposed theory, the transfer matrix for all the time-varying elements can be written independently. Therefore, by cascading the transfer matrices, we will be able to calculate an arbitrary space-time modulation profile. Third, the generalized transfer matrix method provides an interface between time-varying systems and other systems, so it can be used to study the interaction between stationary and nonstationary systems.

C. An acoustic case: Waveguide loaded with space-time-modulated Helmholtz resonators

In this section, we will look into a practical system in acoustics where a waveguide is side loaded with a series of Helmholtz resonators whose cavity heights are modulated in both space and time. The schematic diagram is shown in Fig. 1. Since the resonators are side loaded, such a configuration fits the parallel-load case. The impedance of a Helmholtz resonator can be represented with $Z = j\omega L + \frac{1}{j\omega C}$, where $L = \rho l$, $C = \frac{S_{\rm cav} h}{S_L \rho c^2}$. Here ρ and c are the density and sound speed in air, l is the corrected length of the neck, and S_L and $S_{\rm cav}$ are the area of the neck and cavity, respectively.

Assume the height of the cavity h varies in the form of $h(t) = h_0[1 + m\cos(\Omega t + \phi)]$ and the modulation is weak, i.e., $m \ll 1$. The impedance of a single Helmholtz resonator

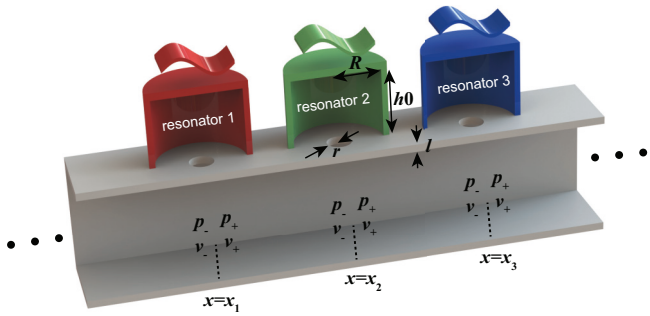

FIG. 1. Schematic representation of a waveguide loaded with an arbitrary number of space-time-modulated resonators

can be written as

$$Z(\omega_n, t) = Z_n\left[1 - \frac{mZ_{cn}}{Z_n}\cos(\Omega t + \phi)\right], \tag{17}$$

where $Z_n = j\omega_n L + \frac{1}{j\omega_n C_0}$, $Z_{cn} = \frac{1}{j\omega_n C_0}$, and $C_0 = \frac{S_{\text{cav}} h_0}{S_L \rho c^2}$ is the acoustic capacitance for a resonator without modulation [14,27,28]. The impedance variation corresponds to the parallel-load case described in Sec. II B. Inserting the impedance into the above formalism, a physical acoustic system can be represented by the transfer matrix framework described above.

III. EXAMPLES IN THE DISCRETIZED SPACE-TIME-MODULATED SYSTEMS

A. Nonreciprocal sound transport

Nonreciprocal devices that create directional control of the energy flow have numerous applications and, consequently, have attracted significant attention in recent years. Nonreciprocal sound transport using space-time modulation was recently reported by cascading modulated resonators [28] or forming a circulator [30,32]. However, the proposed designs require resonators with a high quality factor, and the system has to work close to the resonant frequency. These features bring challenges in realization and make the system sensitive to inevitable losses and fabrication errors. In this section, we will demonstrate the design of a nonreciprocal device by cascading multiple space-time-modulated resonators. Different from the existing strategy that derives the requirements for the resonators, we start from a physically realizable resonator design and then determine the number of resonators needed to generate a sufficient nonreciprocal response at off-resonance frequencies.

For the demonstration of these features, we pick an acoustic waveguide with a cross section of 9.5×9.5 mm^2. The Helmholtz resonator dimension is shown in Fig. 1. The cavity is cylindrical with radius $R = 14$ mm and height $h_0 = 10$ mm. The neck is also cylindrical with radius $r = 4.5$ mm and neck length $l = 1.6$ mm. With the help of a numerical finite-element simulation performed in COMSOL MULTIPHYSICS, we calculated the resonance frequency as 2566 Hz, which yields an effective neck length $l = 4.7$ mm. The distance between adjacent shunted resonators is 40 mm. We would like to note here that the resonator parameters are chosen for demonstrating the capability of the method and not optimizing the device performance. The performance is expected to be improved by further optimization of the geometric parameters, which is not the focus of this paper. Since the calculation deals with slow and weak modulation, we chose the modulation frequency to be 100 Hz and the modulation depth m to be 0.15. The modulation phase of each resonator has a linear gradient; that is, the modulation phase for the nth resonator can be written as $\phi_n = n\Delta\phi$, where $\Delta\phi$ is the phase difference between adjacent resonators. The incident wave is assumed to be sinusoidal with angular frequency ω_0 and is defined as the 0th order. We have studied the same system truncated at different orders and found that for this particular system, the transmission coefficients converge after the $\pm$5th order is considered. The detailed information is summarized in Appendix C. In the study, the waves are truncated to $\pm$10th order.

By multiplying transfer matrices and converting the total transfer matrix into the scattering matrix, the transmission and reflection coefficients for such a system can be calculated. Since we truncated the waves to $\pm$10th order, the size of the scattering matrix is 42 by 42, and $S_{22,21}$ and $S_{21,22}$ represent the transmission coefficients for the 0th-order wave in the forward direction and backward direction (see Appendix B for details). Here we define the transmission ratio $\Gamma = |S_{22,21}|/|S_{21,22}|$ as a measure of the resulting asymmetry. In Fig. 2, we show the change in Γ by varying the phase difference $\Delta\phi$ from $-\pi$ to π and incident frequency from 1000 to 2000 Hz, in the cases of two, three, four, and five cascaded resonators.

With two modulated resonators, the asymmetric modulation creates a directional bias, which leads to nonreciprocity. However, due to the low quality factor of the resonance and the fact that the incident wave is not close to the resonant frequency, the nonreciprocal effect is very weak. In this case, the maximum value of Γ is 1.022 (0.189 dB). As the number of resonators increases, the maximum transmission ratio reaches 1.274 (2.103 dB), 3.585 (11.089 dB), and 51.55 (34.245 dB) with three, four, and five modulated resonators. This indicates that with more resonators which introduce more design degrees of freedom, nonreciprocal transmission can be realized conveniently using this approach.

The analytic model is verified with a one-dimensional (1D) FDTD simulation implemented in MATLAB [38]. The background media is lossless air with density $\rho_0 = 1.21$ kg/m^3 and speed of sound $c_0 = 343$ m/s. The time step is 1×10^{-7} s, and the grid is 5×10^{-5} m. Here we use the four-resonator case as an example. The dimensions for the Helmholtz resonator are the same as the ones we used in the analytic calculation. In the simulation, each of the three-dimensional (3D) resonators is represented by a time-dependent harmonic oscillator, and they couple into the 1D waveguide by inducing the discontinuity in local velocity at each position. As an example, the phase step for each resonator and the incident frequency are chosen to be $\Delta\phi = 0.24\pi$ and 1550 Hz, respectively. The waveguide in front of and behind the structure is 0.5 m, and radiation boundaries are applied to eliminate reflection from both sides. Figure 3 shows the comparison between theoretical calculated transmission coefficients and the simulation results. We can see excellent

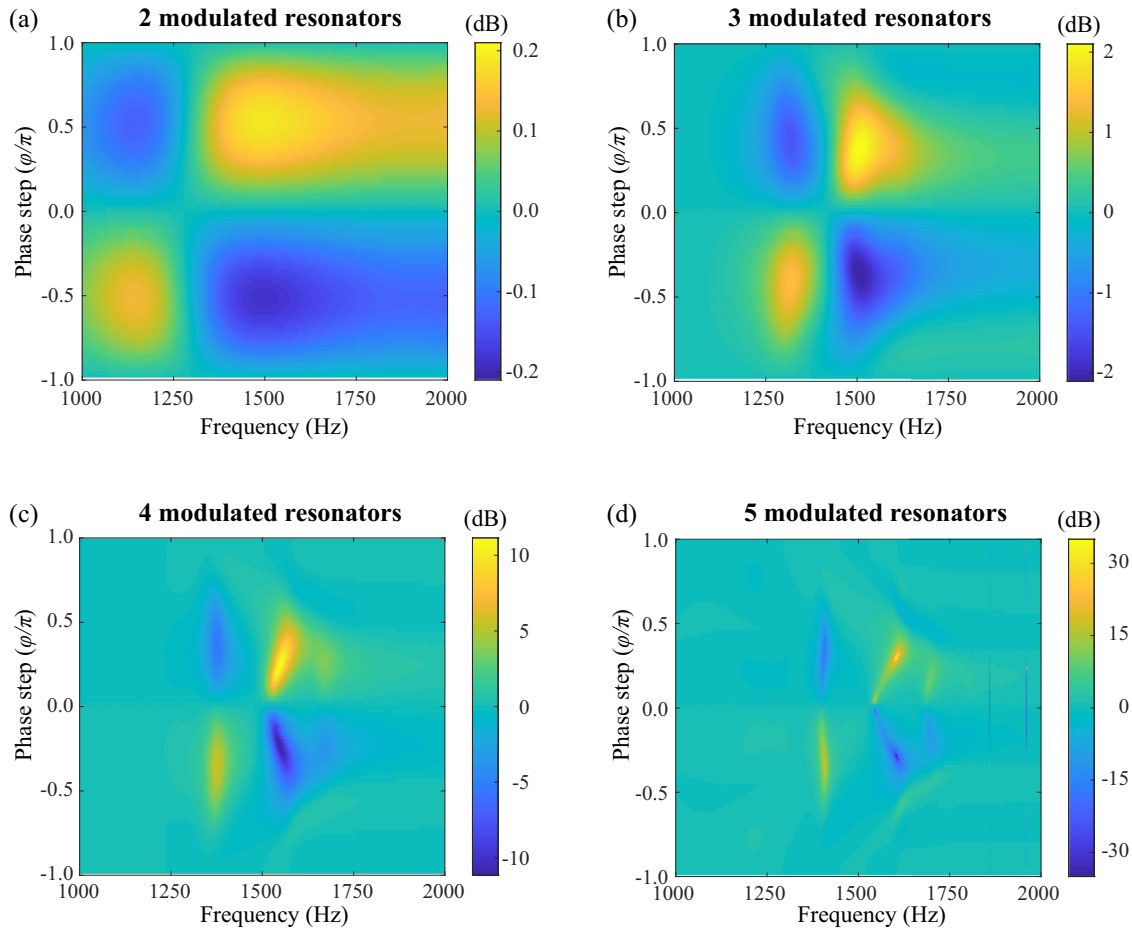

FIG. 2. Transmission ratio for two, three, four, and five space-time-modulated resonators with the change in input frequency and modulation phase step. With the increased number of resonators, the range of available transmission ratio can be increased.

agreement between them where not only the fundamental order but also all the higher-order waves are well captured. The results again confirm that for multiple resonators, higher-order harmonics need to be considered to accurately represent the system. The 0th-order transmission coefficients for the positive direction are 0.2612 and 0.2598 in the calculation and simulation, respectively, and for the negative direction, they are 0.0729 and 0.0860. The small discrepancy may come

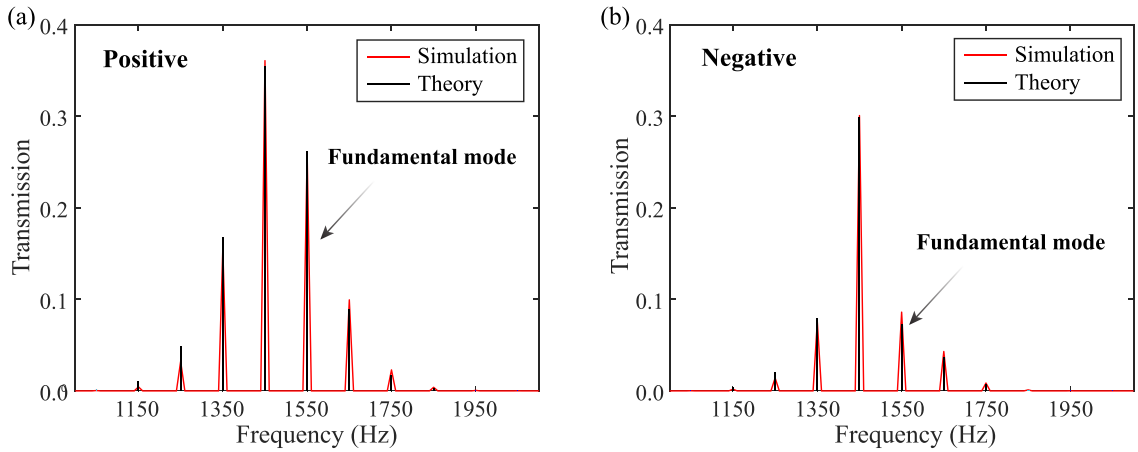

FIG. 3. Comparison of the transmission coefficients for each order between the theoretical calculation and FDTD simulation. The amplitudes of all the involved orders agree well. Nonreciprocal sound transport is achieved at the fundamental frequency of 1550 Hz.

from the first-order truncation in Eq. (17) for the impedance approximation.

B. Parametric frequency conversion and parametric amplification

It has been shown that in TVTLs, parametric frequency conversion and amplification can be achieved if the phase-matching condition is met [1,2,9]. Similar phenomena have also been demonstrated in acousto-optic effects [16,19] and space-time-modulated media [27]. However, the realization of a space-time-modulated effective material usually means approximating a continuous system. In many practical cases, however, it is difficult to discretize the system into deep subwavelength scales. In these cases, multiple scattering may have a significant impact on the wave behavior. Therefore, our theoretical model has a great advantage in characterizing such discretized space-time-varying systems since the scattering is intrinsically built into the model. In this section, we will show that parametric frequency conversion and parametric amplification can be achieved in such a discrete space-time-modulated system. It will also be shown that as we truncate the model to consider only the fundamental mode and targeted mode, the results agree well with those obtained with TVTLs and space-time-modulated metamaterials. On the other hand, as we will discuss in this section, in many cases, high-order modes and multiple reflections have non-negligible effects on the fundamental modes, and therefore, neglecting them will not yield accurate predictions.

The system configuration we use in this section is as follows: the cross section of the acoustic waveguide is 20×20 mm^2; the cavity of the Helmholtz resonator is cylindrical with radius $R = 10$ mm and height $h_0 = 5$ mm, and the neck is also cylindrical with radius $r = 1.5$ mm and effective neck length $l = 3.1$ mm. These parameters yield a resonance frequency of 2091 Hz. Note here that we use a different set of parameters than in the previous case so that the influence of high-order modes and discretization can be better visualized. The distance between adjacent shunted resonators is 40 mm. The modulation depth m is chosen to be 0.15. The effective dispersion curve can be obtained in simulation by effective parameter retrieval [39]. The simulation is done with the commercial finite-element analysis package COMSOL MULTIPHYSICS.

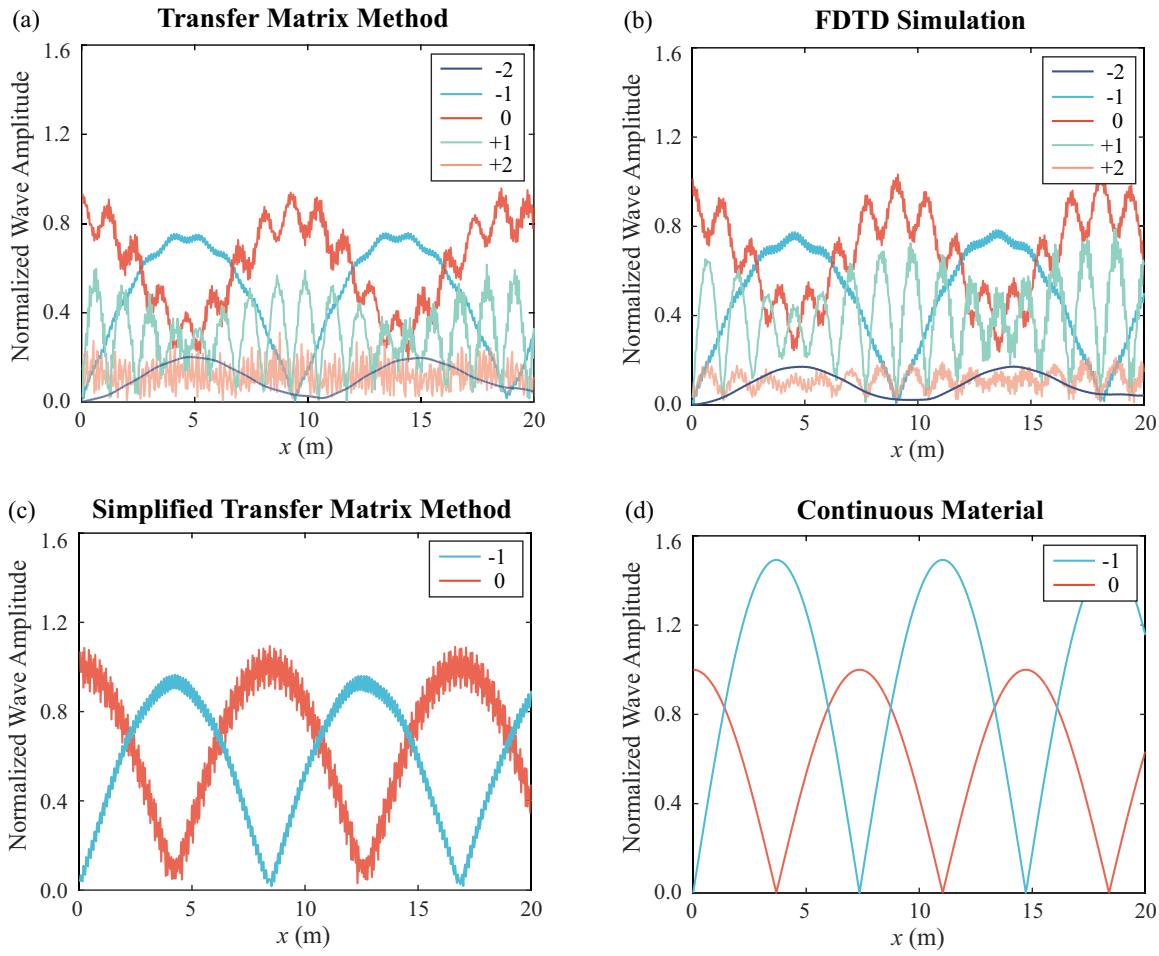

FIG. 4. Comparison between theory and simulation for the case of parametric frequency conversion. (a) The wave amplitudes for 0th- to $\pm$5th-order waves along the waveguide predicted by the transfer matrix method. The calculation truncated at $\pm$10th order. (b) Amplitudes for 0th- to $\pm$5th-order waves obtained from simulation. (c) Wave amplitudes calculated by the transfer matrix method when only 0 and -1 orders are considered, showing that high-order waves have a non-negligible effect. (d) The corresponding calculation using the continuous model as a reference.

The first case we show in this section is the realization of parametric frequency conversion. The total length of the modulated section is 20 m, containing 500 space-time-modulated resonators. Two empty waveguides are connected to both sides of the modulated section. In this case, we use a 1600-Hz wave as the fundamental mode (0th order) and a 1300-Hz wave as the target mode (−1st order). The wave numbers for the two modes are retrieved as $k_1 = 32.69$ rad/m and $k_2 = 25.67$ rad/m. Therefore, the modulation frequency for each resonator is 300 Hz, and the phase step is $\Delta\phi = (k_1 - k_2)\Delta d = 0.28$ rad [27]. Assuming a monochromatic wave (0th order) is incident from the empty waveguide, Fig. 4(a) shows the variation of normalized amplitudes of each mode as the wave propagates along the system. Here the wave amplitudes are obtained by calculating the transmission and reflection coefficients of the space-time-modulated system. This is done by computing the total transfer matrix and converting it to the scattering matrix by assuming air on both sides. Hence, the pressure and velocity for each mode at the incident port can be calculated. By doing this, the interaction between the space-time-modulated system and two empty waveguides can be conveniently analyzed. With total pressure and velocity on the input side, the pressure amplitudes for each order, normalized by the incident wave, at an arbitrary position can be calculated with the help of the transfer matrix. A FDTD simulation is performed to verify the theoretical results. In the simulation, the time step and space step are 1×10^{-7} s and 5×10^{-5} m, respectively. Radiation boundaries are applied on both ends of the empty waveguides to eliminate reflection. The sinusoidal wave is incident from the air section, and we wait 0.4 s for the system to reach its steady state. The waveform along the modulated section from 0.3 to 0.4 s is recorded, and a Fourier transform is performed to analyze its spectrum. Figure 4(b) shows how energy transfers back and forth among the modes while propagating in the system. The simulation results are in good agreement with the theoretical predictions. The theoretically calculated distance needed for one cycle of such a transition is 9.426 m, while in the simulation, the measured distance is 9.069 m. We can see that apart from the incident mode and the target mode, the +1st mode and ±2nd modes all have non-negligible amplitudes. The small oscillation in the amplitudes is a result of interaction with higher-order modes. This can be confirmed by truncating the model to account for only the fundamental mode and the target mode, with all other modes neglected. The mode amplitudes calculated from the simplified model are shown in Fig. 4(c), and we can see that the small oscillation disappears when the high-order modes are turned off. This confirms our conclusion that high-order modes cannot be neglected while treating the time-varying systems. As a comparison, the corresponding results calculated from a continuous effective material model [27] are shown in Fig. 4(d). We can see the energy swapping between two modes, but the amplitudes of two modes are not accurate, and the prediction of the distance needed for a cycle of transition is 7.357 m, which is 18.9% off from the simulation results. This is because in the continuous model, plane wave solutions are assumed. Therefore, with the effective medium approximation, the unit cells are required to be subwavelength. However, this assumption no longer holds near the resonant frequency range, as the wave velocity becomes very slow such that the wavelength is comparable to the spacing between resonators. In our case, the wavelength for the −1st, 0th, and 1st modes are 24.5, 19.2, and 14.1 cm, respectively. They are comparable to the separation of 4 cm and do not satisfy the subwavelength condition. In principle, if the separation is reduced to being infinitesimal, the effective medium approximation will become valid again. However, in practice, it is very hard to achieve due to the following reasons. First, as we have demonstrated above, higher-order harmonics have non-negligible effects on the system performance. To meet the effective medium approximation, the separation has to be much smaller than the smallest wavelength (highest order) taken into account. Second, as the frequency approaches the band gap, the effective sound speed will become extremely slow. Such an effect will make the wavelength even smaller for these frequency ranges, so that the requirement of the effective medium approximation becomes very hard to meet. Therefore, to better predict the wave behavior in a practical system, the Bragg scattering needs to be considered.

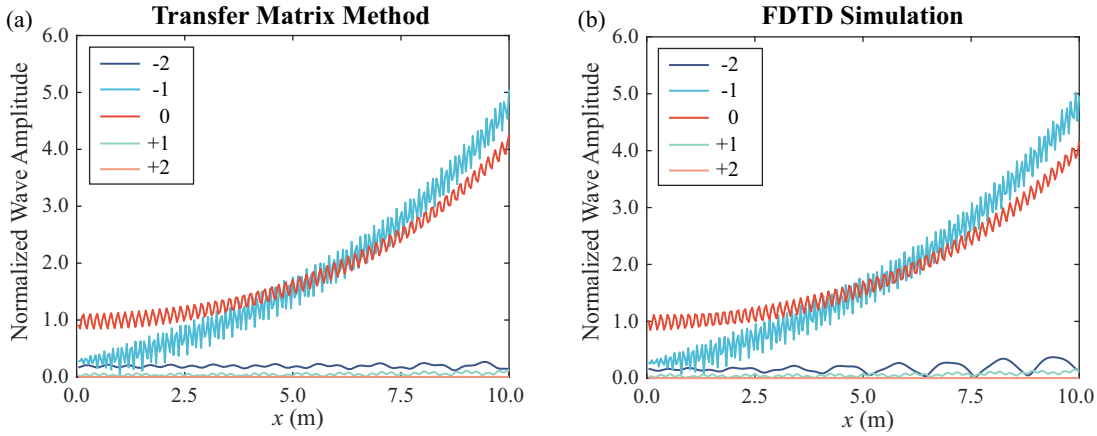

FIG. 5. Comparison between theory and simulation for the case of parametric amplification (non-Hermitian gain media). (a) The wave amplitudes for 0th- to ±2nd-order waves along the waveguide predicted by the transfer matrix method. The calculation truncated at ±10th order. (b) Amplitudes for 0th- to ±2nd-order waves obtained from simulation.

The same resonator geometry is used for the parametric amplification case. To better show how the waves grow gradually, the length of the modulated section is shortened to 10 m. In this case, the modulation frequency is set as 2500 Hz. The frequencies for the incident wave and generated wave are 1000 and 1500 Hz, corresponding to wave numbers $k_1 = 19.46$ rad/m and $k_2 = 30.18$ rad/m, respectively. Therefore, the phase step between each resonator is $\Delta\phi = (k_1 + k_2)\Delta d = 1.99$ rad [27]. The comparison between theory and simulation is given in Fig. 5, where exponential growth for both waves is observed, following the form of $\cosh(\alpha x)$ for the 1000-Hz wave and $\sinh(\alpha x)$ for the 1500-Hz wave, where α represents the growth rate. α is obtained by fitting the data to the function and is found to be 0.2056 and 0.2036 rad/m for theory and simulation, showing excellent agreement. The small oscillation in the growing amplitude is the result of discretization. In both the theoretical calculation and the simulation, the high-order waves are small because these modes are far from the allowed modes in the system, so that the coupling is very weak.

IV. DISCUSSION AND CONCLUSION

In this paper, we proposed a framework to solve one-dimensional wave propagation problems in time-varying acoustic, EM, and IC systems through a generalization of the transfer matrix method. By analyzing the boundary conditions for time-varying impedance in series and in parallel, the boundary conditions can be set up by balancing the harmonics. The boundary condition is converted to a generalized transfer matrix form which facilitates the computation process. With this step, the influence of a time-varying element on the whole system is completely localized. Localization provides the advantage of making the time-varying components serve as individual building blocks and thus allows the study of time-varying systems with complicated modulation profiles by simply multiplying individual pieces.

Compared with currently available models for studying general space-time varying systems, our approach has many advantages. First, it enables the study of complicated spatial modulation strategies instead of simple sinusoidal traveling-wave-like modulation. While dealing with a traveling-wave-like system, it can reduce to the continuous counterpart, such as solving the coupled partial differential equations (as used in TVTLs and space-time-modulated metamaterials) and space-time Floquet theory, with much more precise details. Second, high-order modes are taken into consideration, and we showed the influence of high-order harmonics with two examples: designing a nonreciprocal sound-transporting device and parametric mode conversion. Third, the computational complexity does not grow with the system complexity; therefore, it is effective in studying large systems, while it produces the same results as [28] when the size of the system is small. Fourth, it allows the study of the interaction between space-time-varying behavior and other classical wave behaviors, such as multiple scattering. Fifth, it enables the study of the interaction between a time-varying system and other existing systems and thus offers possibilities for more advanced and complex wave control. Note here that the approach proposed in this paper is a close approximation instead of an accurate result. To the best of our knowledge, there are two main sources for the inaccuracy. The first one is by taking the first term of the Taylor expansion while representing the time-varying impedances; this is valid only when the modulation depth is small enough. The other source of inaccuracy is the truncation of higher-order modes. To predict a system with sufficient accuracy, one should include a sufficient number of modes in the calculation, as illustrated in Appendix C.

Space-time modulation puts a new twist on controlling wave behaviors and opens the door for unprecedented wave manipulation capabilities that are not possible for stationary systems. The possibility offered by modulation is much richer than nonreciprocal wave transport, frequency conversion, and the realization of gain media. It will be important that future research explore richer phenomena enabled by various modulation profiles instead of the simple traveling-wave-like modulation. It will also be beneficial to extend the transfer matrix framework by investigating more complicated modulation waveforms, such as a square wave, sawtooth wave, etc. Additionally, we would like to note that even in a 1D system, there remains a lot of room to explore which requires more insights on the system behaviors under space-time modulation; extension of such a theory into two-dimensional or 3D systems could prove quite beneficial to the literature. We hope this theory will serve as a powerful tool and versatile platform for studying general space-time-modulated systems.

ACKNOWLEDGMENTS

This work was supported by a Multidisciplinary University Research Initiative grant from the Office of Naval Research (Grant No. N00014-13-1-0631) and an Emerging Frontiers in Research and Innovation grant from the National Science Foundation (Grant No. 1641084). X.Z. wishes to acknowledge the China Scholarship Council (CSC) for financial support (Grant No. 201706120133).

APPENDIX A: ELECTROMAGNETIC AND IC FORMULATION OF THE SPACE-TIME-MODULATED SYSTEMS

Here we use TE-polarized EM waves as an example. Assume the $\vec{E}$ field is pointing in the $\hat{x}$ direction and the wave is propagating along the $\hat{z}$ axis. The waves upstream and downstream of a thin impedance sheet connected in series with the waveguide can be written as

$$\vec{E}_{\mp} = \sum_{n=-\infty}^{\infty} \vec{E}_{\mp}^{n} e^{j\omega_n t}, \tag{A1}$$

$$\vec{H}_{\mp} = \sum_{n=-\infty}^{\infty} \vec{H}_{\mp}^{n} e^{j\omega_n t}. \tag{A2}$$

If the impedance sheet has only an electric response and no magnetic response, the boundary conditions for electromagnetic waves can be expressed as

$$\vec{E}_{-} = \vec{E}_{+}, \tag{A3}$$

$$\hat{z} \times (\vec{H}_{+} - \vec{H}_{-}) = \sum_{n=-\infty}^{\infty} Y_L^n \vec{E}_{-}^{n} e^{j\omega_n t}, \tag{A4}$$

TABLE I. Analogy of acoustic, EM, and IC systems and the corresponding realization for series and parallel cases.

	System type	Discontinuity	Realization
Series case	Acoustic	p	Membranes and plates
	EM	$\vec{E}$	Impedance sheets that create magnetic current
	IC	V	Impedance in series
Parallel case	Acoustic	v	Side-loaded resonators
	EM	$-\hat{n}\times\vec{H}$	Impedance sheets that create electric current
	IC	I	Impedance in parallel

where Y_L is the admittance of the sheet. Now if we assume the admittance varies in the form of $Y_L(\omega)=Y_{L0}(\omega)[1+a\cos(\Omega t+\phi)]$, the boundary conditions for each order then become

$$\vec{E}_-^n=\vec{E}_+^n, \tag{A5}$$

$$(-\hat{z}\times\vec{H}_-^n)-(-\hat{z}\times\vec{H}_+^n)=Y_{L0}^n\vec{E}_-^n+\frac{aY_{L0}^{n-1}}{2}e^{j\phi}\vec{E}_-^{n-1}+\frac{aY_{L0}^{n+1}}{2}e^{-j\phi}\vec{E}_-^{n+1}. \tag{A6}$$

Comparing Eqs. (A3) and (A4) and Eqs. (12) and (13), we can see that they take the same form, where $\vec{E}$ corresponds to p and $-\hat{z}\times\vec{H}$ corresponds to v. This corresponds to the parallel impedance case in acoustics. By converting these equations into the transfer matrix form, all the field terms will be isolated, so that the transfer matrix is exactly the same as the one we derived in Eq. (16). Similar equations can be found for an impedance sheet with time-varying magnetic responses.

For IC systems, the analogy is straightforward. By replacing p with V and v with I, all the matrices can be obtained and remain in the same form as in the acoustic formulation. Here V and I denote voltage and current.

The analogy of acoustic, EM, and IC systems in the series case and parallel case and the corresponding realization approaches are summarized in Table I.

APPENDIX B: CONVERSION FROM TRANSFER MATRIX TO SCATTERING MATRIX

The schematic diagram is shown in Fig. 6. The transfer matrix and scattering matrix of the structure are defined as

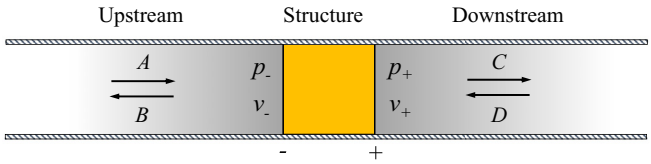

FIG. 6. Schematic of the system for matrix conversion.

$$\begin{bmatrix}\vdots\\ p_-^{n-1}\\ v_-^{n-1}\\ p_-^{n}\\ v_-^{n}\\ p_-^{n+1}\\ v_-^{n+1}\\ \vdots\end{bmatrix}=M\begin{bmatrix}\vdots\\ p_+^{n-1}\\ v_+^{n-1}\\ p_+^{n}\\ v_+^{n}\\ p_+^{n+1}\\ v_+^{n+1}\\ \vdots\end{bmatrix}, \tag{B1}$$

$$\begin{bmatrix}\vdots\\ B^{n-1}\\ C^{n-1}\\ B^{n}\\ C^{n}\\ B^{n+1}\\ C^{n+1}\\ \vdots\end{bmatrix}=S\begin{bmatrix}\vdots\\ A^{n-1}\\ D^{n-1}\\ A^{n}\\ D^{n}\\ A^{n+1}\\ D^{n+1}\\ \vdots\end{bmatrix}. \tag{B2}$$

The calculation strategy of the transfer matrix is given in Sec. II and can be expressed as

$$M=\begin{bmatrix}&\vdots&\vdots&\vdots&\\ \cdots&M'_{n-1,n-1}&M'_{n-1,n}&M'_{n-1,n+1}&\cdots\\ \cdots&M'_{n,n-1}&M'_{n,n}&M'_{n,n+1}&\cdots\\ \cdots&M'_{n+1,n-1}&M'_{n+1,n}&M'_{n+1,n+1}&\cdots\\ &\vdots&\vdots&\vdots&\end{bmatrix}, \tag{B3}$$

where

$$M'_{i,j}=\begin{bmatrix}M_{2i-1,2j-1}&M_{2i-1,2j}\\ M_{2i,2j-1}&M_{2i,2j}\end{bmatrix}. \tag{B4}$$

Using A^n, B^n, C^n, and D^n to represent p_-^n, v_-^n, p_+^n, and v_+^n, we can rewrite Eq. (B1) as

$$\begin{bmatrix} & \vdots & \vdots & \vdots & \\ \cdots & S^{\text{out}}_{n-1,n-1} & S^{\text{out}}_{n-1,n} & S^{\text{out}}_{n-1,n+1} & \cdots \\ \cdots & S^{\text{out}}_{n,n-1} & S^{\text{out}}_{n,n} & S^{\text{out}}_{n,n+1} & \cdots \\ \cdots & S^{\text{out}}_{n+1,n-1} & S^{\text{out}}_{n+1,n} & S^{\text{out}}_{n+1,n+1} & \cdots \\ & \vdots & \vdots & \vdots & \end{bmatrix} \begin{bmatrix} \vdots \\ \text{Out}^{n-1} \\ \text{Out}^{n} \\ \text{Out}^{n+1} \\ \vdots \end{bmatrix} = \begin{bmatrix} & \vdots & \vdots & \vdots & \\ \cdots & S^{\text{in}}_{n-1,n-1} & S^{\text{in}}_{n-1,n} & S^{\text{in}}_{n-1,n+1} & \cdots \\ \cdots & S^{\text{in}}_{n,n-1} & S^{\text{in}}_{n,n} & S^{\text{in}}_{n,n+1} & \cdots \\ \cdots & S^{\text{in}}_{n+1,n-1} & S^{\text{in}}_{n+1,n} & S^{\text{in}}_{n+1,n+1} & \cdots \\ & \vdots & \vdots & \vdots & \end{bmatrix} \begin{bmatrix} \vdots \\ In^{n-1} \\ In^{n} \\ In^{n+1} \\ \vdots \end{bmatrix}, \tag{B5}$$

where

$$\text{Out}^n = \begin{bmatrix} B^n \\ C^n \end{bmatrix}, \tag{B6}$$

$$\text{In}^n = \begin{bmatrix} A^n \\ D^n \end{bmatrix}, \tag{B7}$$

$$S^{\text{out}}_{i,j} = \begin{bmatrix} \delta_{ij} & -\left(M'_{i,j}(1,1) + \dfrac{M'_{i,j}(1,2)}{z_0}\right) \\ -\dfrac{\delta_{ij}}{z_0} & -\left(M'_{i,j}(2,1) + \dfrac{M'_{i,j}(2,2)}{z_0}\right) \end{bmatrix}, \tag{B8}$$

$$S^{\text{in}}_{i,j} = \begin{bmatrix} -\delta_{ij} & \left(M'_{i,j}(1,1) - \dfrac{M'_{i,j}(1,2)}{z_0}\right) \\ -\dfrac{\delta_{ij}}{z_0} & \left(M'_{i,j}(2,1) - \dfrac{M'_{i,j}(2,2)}{z_0}\right) \end{bmatrix}. \tag{B9}$$

δ_{ij} is the Kronecker delta. Then, we can get the scattering matrix of the structure as

$$S = [S^{\text{out}}]^{-1} S^{\text{in}}. \tag{B10}$$

From the definition of the scattering matrix [Eq. (B2)], we can see that the transmission and reflection coefficients for each order can be directly obtained from the corresponding elements in the scattering matrix. For simplicity, we represent the scattering matrix as

$$S = \begin{bmatrix} & \vdots & \vdots & \vdots & \\ \cdots & S'_{n-1,n-1} & S'_{n-1,n} & S'_{n-1,n+1} & \cdots \\ \cdots & S'_{n,n-1} & S'_{n,n} & S'_{n,n+1} & \cdots \\ \cdots & S'_{n+1,n-1} & S'_{n+1,n} & S'_{n+1,n+1} & \cdots \\ & \vdots & \vdots & \vdots & \end{bmatrix}, \tag{B11}$$

where

$$S'_{i,j} = \begin{bmatrix} r^+_{i,j} & t^-_{i,j} \\ t^+_{i,j} & r^-_{i,j} \end{bmatrix}, \tag{B12}$$

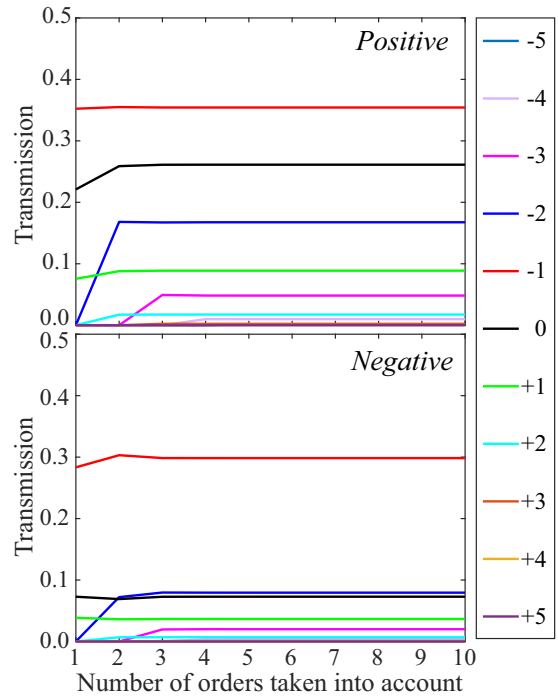

FIG. 7. Transmission coefficients for 0th- to ±5th-order modes as we increase the number of orders taken into account. The upper and lower figure are the scenario when the incident wave is from the positive direction and the negative direction, respectively. The results remain unaffected after accounting for the ±5 order.

where each element in $S'_{i,j}$ represents the reflection and transmission coefficients for the positive direction and negative direction, corresponding to the ith-order output and jth-order input.

APPENDIX C: CONVERGENCE OF THE RESULTS AS MORE ORDERS ARE TAKEN INTO ACCOUNT

One of the main advantages for our proposed method is that it takes high-order waves into account. Then it comes to the question of what kind of truncation gives reliable results. Here we pick the four-resonator nonreciprocal sound transmission case as an example. Figure 7 shows the convergence of transmission coefficient amplitudes for 0th- to ±5th-order waves as we increase the number of modes taken into account during the truncation process. Here the transmission coefficient for each order is defined as the ratio between the complex amplitude for each order and the incident wave amplitude. They can be directly obtained from the corresponding components in the scattering matrix. From Fig. 7 we can see that high-order harmonics do play a role, and sometimes they are higher than the 0th order; therefore, omitting them during the calculation will lead to inaccurate results. In our example case, the amplitudes of harmonics higher than ±5th order are lower than 0.01 and therefore can be neglected. The amplitudes of the 0th to ±5th orders remain essentially unchanged after the 5th order is taken into account. This justifies our calculation where we truncated the matrix at ±10th order.

[1] P. Tien and H. Suhl, Proc. IRE **46**, 700 (1958).
[2] P. Tien, J. Appl. Phys. **29**, 1347 (1958).
[3] A. Cullen, Nature (London) **181**, 332 (1958).
[4] J.-C. Simon, IRE Trans. Microwave Theory Tech. **8**, 18 (1960).
[5] A. Oliner and A. Hessel, IRE Trans. Microwave Theory Tech. **9**, 337 (1961).
[6] E. Cassedy and A. Oliner, Proc. IEEE **51**, 1342 (1963).
[7] E. Cassedy, Proc. IEEE **55**, 1154 (1967).
[8] C. Elachi, IEEE Trans. Antennas Propag. **20**, 534 (1972).
[9] S. Qin, Q. Xu, and Y. E. Wang, IEEE Trans. Microwave Theory Tech. **62**, 2260 (2014).
[10] H. Lira, Z. Yu, S. Fan, and M. Lipson, Phys. Rev. Lett. **109**, 033901 (2012).
[11] M. Hafezi and P. Rabl, Opt. Express **20**, 7672 (2012).
[12] D. L. Sounas and A. Alù, ACS Photonics **1**, 198 (2014).
[13] N. A. Estep, D. L. Sounas, J. Soric, and A. Alù, Nat. Phys. **10**, 923 (2014).
[14] Y. Hadad, D. L. Sounas, and A. Alu, Phys. Rev. B **92**, 100304(R) (2015).
[15] D. Correas-Serrano, J. Gomez-Diaz, D. Sounas, Y. Hadad, A. Alvarez-Melcon, and A. Alù, IEEE Antennas Wireless Propag. Lett. **15**, 1529 (2016).
[16] F. Ruesink, M.-A. Miri, A. Alu, and E. Verhagen, Nat. Commun. **7**, 13662 (2016).
[17] Y. Hadad, J. C. Soric, and A. Alu, Proc. Natl. Acad. Sci. USA **113**, 3471 (2016).
[18] S. Taravati and C. Caloz, IEEE Trans. Antennas Propag. **65**, 442 (2017).
[19] M.-A. Miri, F. Ruesink, E. Verhagen, and A. Alù, Phys. Rev. Appl. **7**, 064014 (2017).
[20] Y. Shi, Q. Lin, M. Minkov, and S. Fan, IEEE J. Sel. Top. Quantum Electron. **24**, 3500107 (2018).
[21] A. Y. Song, Y. Shi, Q. Lin, and S. Fan, Phys. Rev. A **99**, 013824 (2019).
[22] S. Y. Elnaggar and G. N. Milford, arXiv:1901.08698.
[23] G. Trainiti and M. Ruzzene, New J. Phys. **18**, 083047 (2016).
[24] G. Trainiti, Y. Xia, J. Marconi, G. Cazzulani, A. Erturk, and M. Ruzzene, Phys. Rev. Lett. **122**, 124301 (2019).
[25] H. Nassar, H. Chen, A. Norris, M. Haberman, and G. Huang, Proc. R. Soc. A **473**, 20170188 (2017).
[26] Y. Wang, B. Yousefzadeh, H. Chen, H. Nassar, G. Huang, and C. Daraio, Phys. Rev. Lett. **121**, 194301 (2018).
[27] J. Li, C. Shen, X. Zhu, Y. Xie, and S. A. Cummer, Phys. Rev. B **99**, 144311 (2019).
[28] C. Shen, J. Li, Z. Jia, Y. Xie, and S. A. Cummer, Phys. Rev. B **99**, 134306 (2019).
[29] R. Fleury, D. L. Sounas, C. F. Sieck, M. R. Haberman, and A. Alù, Science **343**, 516 (2014).
[30] R. Fleury, D. L. Sounas, and A. Alù, Phys. Rev. B **91**, 174306 (2015).
[31] T. T. Koutserimpas and R. Fleury, Wave Motion **89**, 221 (2019).
[32] R. Fleury, A. B. Khanikaev, and A. Alu, Nat. Commun. **7**, 11744 (2016).
[33] G. Floquet, Ann. Ec. Norm. Super. **12**, 47 (1883).
[34] A. Yariv, IEEE J. Quantum Electron. **9**, 919 (1973).
[35] H. A. Haus and W. Huang, Proc. IEEE **79**, 1505 (1991).
[36] Q. Li, T. Wang, Y. Su, M. Yan, and M. Qiu, Opt. Express **18**, 8367 (2010).
[37] D. M. Pozar, *Microwave Engineering* (Wiley, Hoboken, NJ, 2009).
[38] D. M. Sullivan, *Electromagnetic Simulation Using the FDTD Method* (Wiley, Hoboken, NJ, 2013).
[39] D. R. Smith, D. C. Vier, T. Koschny, and C. M. Soukoulis, Phys. Rev. E **71**, 036617 (2005).